Effect of high-energy ball-milling on the magnetostructural properties of a $Ni_{45}Co_5Mn_{35}Sn_{15}$ alloy

J. López-García[1,2 *], V. Sánchez-Alarcos[1,2], V. Recarte[1,2], J. A. Rodríguez-Velamazán[3], I. Unzueta[4,5], J. A. García[6], F. Plazaola[6], P. La Roca[1,2,7], J. I. Pérez-Landazábal[1,2].

[1]Department of Physics, Universidad Pública de Navarra, Campus de Arrosadia, 31006 Pamplona, Spain
[2]Institute for Advanced Materials (INAMAT), Universidad Pública de Navarra, Campus de Arrosadia, 31006 Pamplona, Spain
[3]Institut Laue-Langevin, 71 Avenue des Martyrs, 38000 Grenoble, France

[4]Department of Applied Mathematics, University of the Basque Country UPV/EHU, 48013, Bilbao, Spain
[5]BCMaterials, University of the Basque Country UPV/EHU, 48940, Leioa, Spain
[6]Department of Applied Physics II, University of the Basque Country UPV/EHU, 48940, Leioa, Spain

[7]Centro Atómico Bariloche (CNEA), CONICET, Bariloche 8400, Argentina.

* Corresponding author

E-mail adress: javier.lopezg@unavarra.es

Abstract

The effect of high-energy ball-milling on the magnetostructural properties of a $Ni_{45}Co_5Mn_{35}Sn_{15}$ alloy in austenitic phase at room temperature has been analyzed by neutron and high-resolution X-ray diffraction. The ball milling promotes a mechanically-induced martensitic transformation as well as the appearance of amorphous-like non-transforming regions, following a double stage; for short milling times (below 30 minutes), a strong size reduction and martensite induction occur. On the opposite, for longer times, the increase of strains predominates and consequently a larger amount of non-transforming regions appears. The effect of the microstructural defects brought by milling (as dislocations) on both the enthalpy change at the martensitic transformation and the high field magnetization of the austenite has been quantitatively estimated and correlated to the internal strains. Contrary to what occurs in ternary Ni-Mn-Sn alloys, the mechanically-induced defects do not change the ferromagnetic coupling between Mn atoms, but just cause a net reduction on the magnetic moments.

Keyword: Metamagnetic shape memory alloy, high-energy ball-milling, microstructural defects, neutron diffraction

INTRODUCTION

Ni-Mn-Z (Z=In, Sn, and Sb) metamagnetic shape memory alloys (MSMA) have received much attention due to the exceptional properties they show as a result of the coupling

between magnetism and crystal structure [1]. In particular, these alloys show a large variation on the magnetization (ΔM) associated with the occurrence of a first order martensitic transformation (MT) between ferromagnetic austenite and weak-magnetic martensite. The large ΔM across the structural transformation makes the induction of the reverse MT possible by the application of a magnetic field [2–7]. Due to the different magnetic features of the structural phases, such magnetically-induced transformation may give rise to a very large inverse magnetocaloric effect (MCE) [8–13] or to giant magnetoresistance (GMR) [14–16], thus making these materials very attractive for magnetic refrigeration and sensing applications.

The MT characteristics and the magnetic properties (and therefore the functional properties) of these alloys can be tuned by varying the composition of the alloy [4, 17–25], changing the long-range atomic order through thermal treatments [26–29] or modifying the microstructure of the alloy [30–34]. The effect of composition on the magnetostructural properties has been widely analyzed and complete structural and magnetic phase diagrams have been established [18, 20, 35, 36]. Concerning compositional variations, it has been shown that doping the alloy with Co enhances the magnetism of the austenite, thus increasing the ΔM associated to the MT and therefore giving rise to larger magnetically-induced shifts of the MT temperatures and higher associated magnetocaloric effect [2, 13, 37–39]. In particular, in Co-doped Ni-Mn-Sn alloys, the magnetic coupling between the Mn moments on the 4*a* and 4*b* sites changed from being antiferromagnetic to ferromagnetic by substitution of Co [37]. In Ni-Mn-In alloy, in turn, the magnetic coupling between Mn atoms is initially ferromagnetic, but the substitution of Ni by Co produces an increment of the 4*b* local magnetic moment that enhances the magnetism of the austenite [29].

On the other hand, it has been shown that the magnetostructural properties of Ni-Mn-In and Ni-Mn-In-Co alloys can be properly tuned varying the long-range atomic order whereas in the Ni-Mn-Sn system the high stability of the $L2_1$ structure precludes the modification of atomic order by means of conventional thermal treatments [40]. In this latter alloys, the modification of microstructural parameters appears as the only way to modify the functional properties for a selected alloy composition. The influence of mechanically-induced defects on the magnetostructural properties has been recently analyzed in Ni-Mn-Sn and Ni-Mn-Sn-Co alloys subjected to hand-crushing and subsequent annealing treatments [31, 32, 41]. In ternary alloys it has been found that even though no atomic disorder is induced by milling, the antiphase boundaries linked to dislocations promote the antiferromagnetic coupling of Mn, thus resulting in a significant decrease in the saturation magnetization [31]. Further relaxation processes brought by annealing lead to the recovery of the martensitic transformation and the enhancement of the magnetism. In Co-doped alloy, in turn, the different exchange coupling between nearest neighbors Mn atoms in the austenitic and in the martensitic structures produces an increase of the magnetization variation at the MT as a result of the presence of defects, which means that, far for worsening, the presence of defects may be beneficial for MCE applications.

Apart from fundamental considerations, the study of microstructure and microstructural defects has special relevance in the mechanical production of micro and nanoparticles. This is an interesting issue as long as composites consisting of a ductile polymer matrix with MSMA in powder (where the polymer provides integrity and the MSMA the functionality) have been recently proposed and developed to overcome the intrinsic brittleness of the bulk alloys [42–

47]. Likewise, a controlled powder production is also crucial for bed binder jetting or similar 3D printing techniques, which are currently being considered as an alternative for the elaboration of different and complex geometry shape memory alloys-based devices [48–50]. In this sense, a previous and complete characterization of the powder alloys is needed.

Ball milling is an easy and cost-effectiveness method to both induce microstructural defects and reduce the particle size [51]. Previous studies on ternary Ni-Mn-Sn alloys have revealed that, in general, milling leads to a reduction in the crystalline grain size concomitantly with defect inclusions in the crystalline lattice [30, 52]. This results in a decrease of both the ferromagnetic exchange interaction contribution and the magnetic entropy change at the MT, which, in turn, can be enhanced upon proper annealing treatments. Nevertheless, up to now, no similar study has been carried out in Ni-Mn-Sn-Co alloys, in which the presence of microstructural defects has been proved to be beneficial, at least for soft milling. In this respect, in the present work, a systematic study of the effect of high-energy ball-milling on the magnetostructural properties of a $Ni_{45}Co_5Mn_{35}Sn_{15}$ alloy (the same alloy studied in [41]) is performed. Using neutron and synchrotron X-ray diffraction, electron microscopy, differential scanning calorimetry and SQUID magnetometry, the evolution of the microstructural parameters has been quantified and correlated to the evolution of the MT features and the magnetic properties. Apart from the expected grain size reduction, it is found that microstural defects induced during milling cause a reduction of the magnetic moment both in martensite and austenite. The induction of martensitic phase and the partial amorphization of the alloys as a consequence of milling also contribute to the decrease of both the saturation magnetization and the magnetic entropy change at the MT. Opposite to what found in hand-crushed samples, in the present case milling seems to be highly detrimental for the functional properties of the alloy.

EXPERIMENTAL PROCEDURE

A $Ni_{45}Co_5Mn_{35}Sn_{15}$ alloy was synthesized from high purity elements by arc-melting under a protective argon atmosphere. The obtained bulk was remelted five times and homogenized at 1173 K for 24h under argon atmosphere and slowly cooled to room temperature (RT). The composition was analyzed by EDS in a Jeol JSM-5610LV Scanning Electron Microscope (SEM) and the obtained images from secondary electron micrographs were analyzed by the Image-J program [53]. To prepare the sample for ball-milling, the alloy was subjected to hand milling in an agate mortar until reaching a uniform particle-size distribution as previously reported [41]. To analyze the microstructure evolution, a systematic ball milling was performed at RT and at different milling times (15, 30, 45, 60, 90 minutes) in a RETSCH EMAX with a ball-to-powder ratio of 5:1 at 800 rpm under argon atmosphere and controlled temperature, avoiding the possibility of oxidation. Both drams and balls are made of Tungsten Carbide. It is worth noting that the MT of the hand milled powder takes place well below RT [41], in such a way that the ball milling is performed at least initially in the austenitic phase. The MT was characterized by differential scanning calorimetry (Q-100 DSC, TA Instruments), by heating-cooling cycle performed between 140 K and 300 K at 10 K/min. The macroscopic magnetic characterization of the alloys was performed by SQUID magnetometry (QD MPMS

XL-7); measurements of the FC-FH temperature dependence of magnetization between 10 K and 400 K (at 2 K/min under 100 Oe and 60 kOe) and magnetization dependence on the applied magnetic field at 10 K and 300 K. The neutron scattering experiments were carried out at Institut Laue-Langevin, in Grenoble, France. Crystallographic and magnetic structures were analyzed by powder neutron diffraction, using data collected in D1B (λ=1.28Å). For the analysis of microstructural parameters such as crystallite size and internal strains, High-Resolution X-rays Powder Diffraction (HRXPD) was carried out in the BL04_MPSD beamline (28keV) at ALBA synchrotron, Barcelona, Spain using a high-resolution detector (mad26) [54, 55]. Diffraction data treatment was carried out using the programs of the Fullprof Suite [56].

RESULTS AND DISCUSSION

Figure 1a-e shows the SEM micrographs of the milled samples. As expected, the particle size decreases with the increasing milling time. In particular, the average particle size decreases from 65 μm, for the sample milled for 15 minutes, to around 13 μm, for the sample milled for 60 min. Likewise, the size distribution gets more homogeneous with the increase of milling time as shown by the reduction of the width of the histograms. Nevertheless, it is worth noting the presence of abnormally large particles after 90 minutes, probably as a consequence of the agglomeration of small particles or as an effect of cold welding [57, 58]. The evolution of the average particle size with the milling time is shown in Figure 1d.

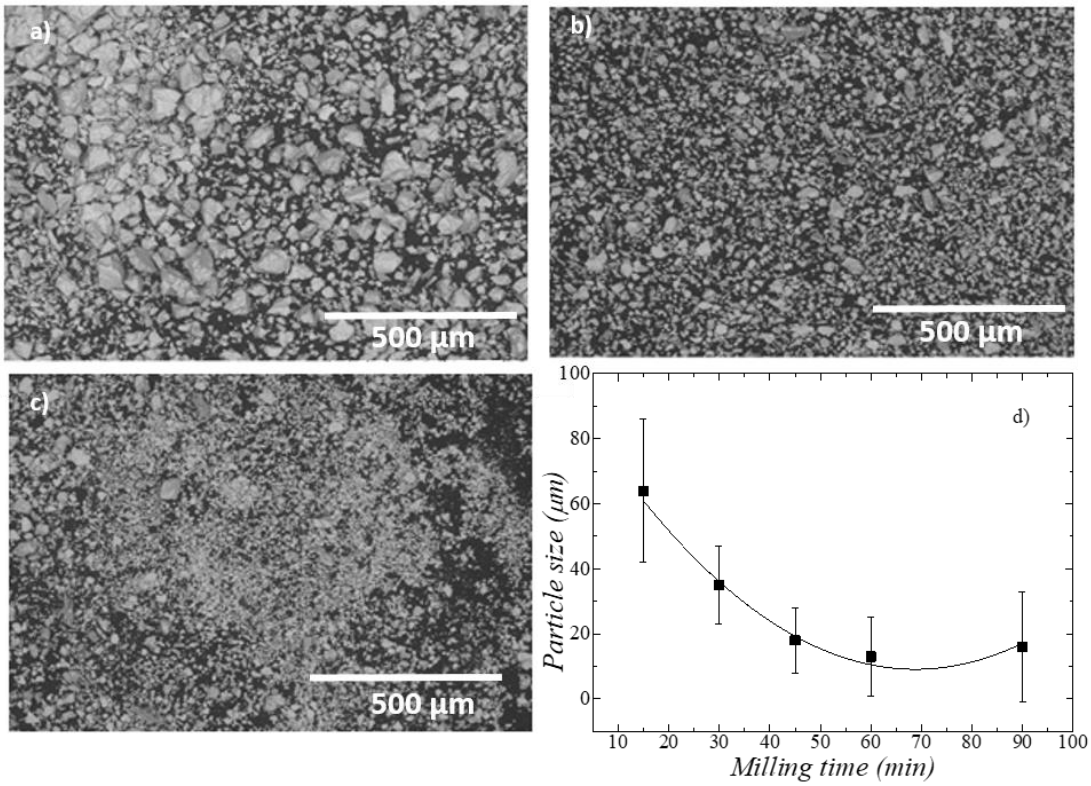

Figure 1. SEM images and particle size histograms for the obtained powder after milling a)15 min, b) 45 min, c) 60 min, and d) average particle size as a function of the milling time.

The occurrence of the MT in the powders and its thermodynamical characteristics have been analyzed from DSC measurements. Figure 2 shows the heating curve of DSC thermograms performed between 140 K and 300 K. The endothermic peaks observed around 190 K correspond to the reverse MT. Similar exothermic peaks corresponding to the forward MT (not shown here for the sake of clarity) are observed on cooling around 150 K. Interestingly, the MT temperature does not evolve with the milling time. Taking into account the high sensibility of these transition temperatures to long-range atomic order [26, 28], the absence of evolution suggests a scarce effect of milling on the atomic order, as it could be indeed expected given the high stability of the $L2_1$ structure in the Ni-Mn-Sn system [40]. However, the area of the transformation peak significantly decreases with the increase of milling time. This points out a clear degradation of the MT, which indeed vanishes for milling times above 45 minutes. A monotonous increase of the volume fraction of non-transforming regions with the milling time can be inferred from the evolution of the heat exchange at the reverse MT (see inset).

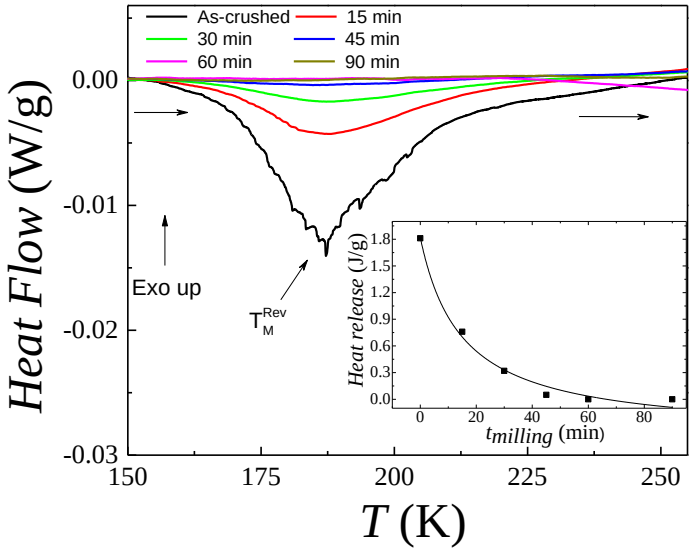

Figure 2. DSC curves on heating at 10 K/min on the studied samples (inset: variation of heat relased with the milling time).

High-energy X-ray powder diffraction measurements (28 keV - λ =0.4424 Å) were performed to analyze the crystallographic structures and the microstructural parameters of the milled samples. Figure 3 shows the diffractograms obtained above and below the MT (RT and 80 K, respectively). At room temperature (Figure 3a), all the samples seem to display a similar $L2_1$ cubic structure with a small reduction of the lattice parameters evolving from 5.977(1) Å to 5.966(2) Å for the as-crushed sample and the powder milled for 90 minutes, respectively. The most evident consequences of milling on the diffractograms are the decrease of the intensity and the widening of the diffraction peaks. This behavior can be typically ascribed to both the grain size reduction and the increase of internal strains linked to microstructural defects like dislocations or antiphase boundaries. Nevertheless, the gradual blurring of the peaks shape and the disappearance of several Bragg reflections also point to the presence of strongly deformed amorphous-like non transforming regions (NTR), whose volume fraction would increase with the milling time. Furthermore, focusing on the (220) reflection of the austenitic structure, a

small peak corresponding to the (200) reflection of the *I2/m* monoclinic martensite is clearly distinguished, pointing out to the induction of martensite at RT as another consequence of milling (Figure 3b). A significant increase of the fraction of induced martensite can be inferred from the increase of the intensity of the martensitic reflection (at the expense of the austenitic one) with the milling time. It is worth mentioning that neither the induction of martensite nor the presence of NTRs have been previously reported and quantified in ternary Ni-Mn-Sn alloys, subjected to even longer milling times [34], so it could be assume as a consequence of the Co doping.

Concerning the low temperature structures, at 80 K (Figure 3c) all the samples show the same monoclinic martensitic structure together with a varying small percentage of retained austenite. The gradual peak broading due to the presence of NTR is also clearly observed.

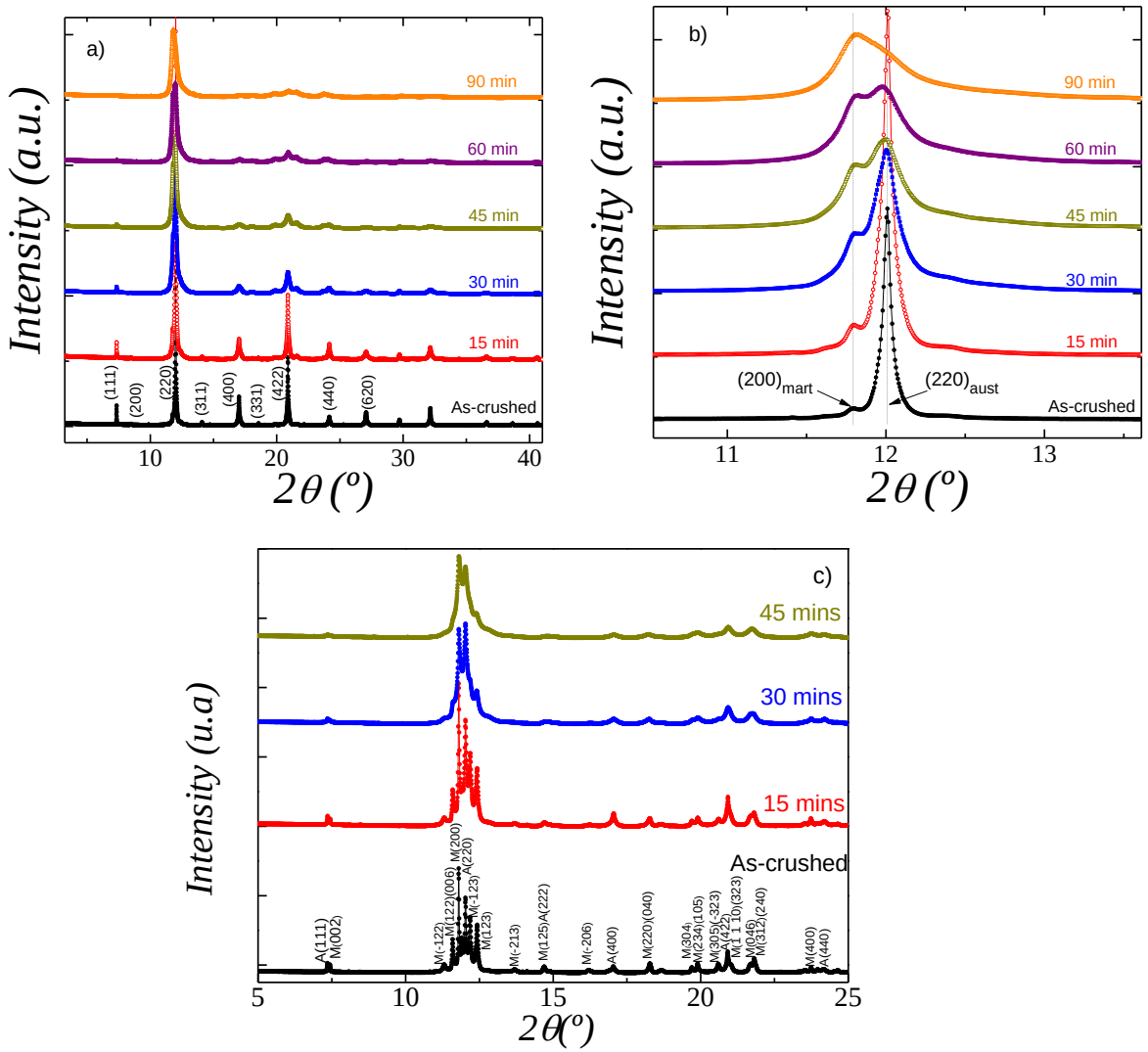

Figure 3. (a) X-ray diffractograms at room temperature for the samples studied in this section. (b) Detail of the region around the most intense reflection of the austenite phase (2 2 0) showing the appearance of a peak corresponding to the martensitic phase. (c) X-ray diffractograms at 80K for as-crushed and the sample milled for 15, 30, and 45 minutes.

Crystallite size and internal strains on the powder samples have been estimated from Lebail fit of the RT diffractograms. As expected, the crystallite size decreases and the internal strains increase with the increasing milling time (Figure 4). After an initial sudden size decrease, a nearly saturated value is reached after 30 minutes. For longer times, milling seems to be not effective in reducing the crystallite size (as it occurred with the particle size, see Fig 1). In fact, the biggest change in the internal strains takes place between 30 and 45 minutes, once the size is no longer reduced and the sample just becomes more deformed with the milling time.

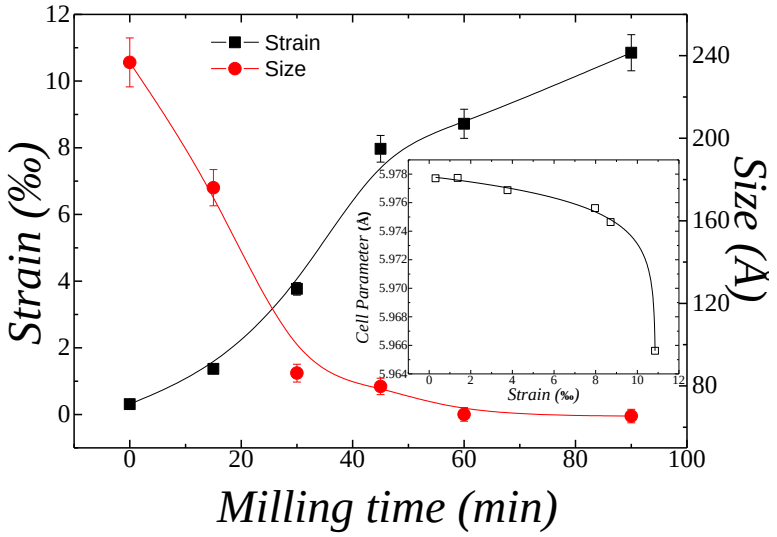

Figure 4. Evolution of average microstrains and crystallite size with the time of milling (inset: cell parameter evolution with the microstrains). Lines are guide for eyes.

The mass fractions of austenite, martensite and NTR present in the alloy after the different milling times have been evaluated from the diffraction patterns using Rietveld method (see figure 5). In order to estimate its mass fraction, an A2 crystal structure (space group $Im\bar{3}m$) has been assigned to the NTR, this crystal structure showing the maximum atomic disorder compatible with the austenitic cubic structure (the lattice parameter of the A2 structure taken as half that of the $L2_1$ austenitic structure) [59, 60]. At room temperature, the fraction of induced martensite continuously increases with the milling time, reaching a saturation value of around 20% for 45 minutes. In turn, the fraction of NTR slightly increases for milling times up to 30 minutes and then a large increase takes place concurrent with the end of the martensite induction. As a consequence of the increase of martensite and NTR at RT, a drastic decrease (around 80%) on the amount of austenite is observed. On the other hand, as previously mentioned, some retained austenite is present at 80 K. The fraction of retained austenite also increases with the milling time, probably linked to the increase of plastically deformed regions that inhibit the MT. From the evolutions shown in Figures 4 and 5, two different stages may be distinguished as a function of the milling time: grain size reduction and martensite induction for milling times below 30 minutes, and plastic deformation leading to pseudoamorphization (and the corresponding increase of internal strains) for longer milling times.

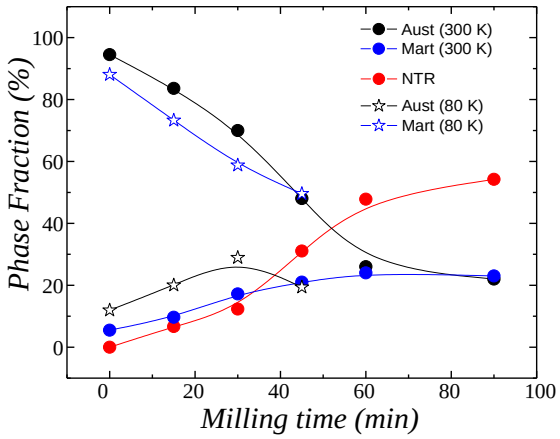

Figure 5. Evolution of phase fractions of austenite, induced martensite, and NTR phase with milling time at room temperature and 80K.

So, the percentage of sample undergoing the MT, calculated as the difference between the austenite fraction at 300 K, the NTR and the austenite fraction at 80 K, highly decreases with the milling time since neither the induced martensite nor the NTR transform on cooling from RT (see figure 6a). Now, the intrinsic enthalpy change at the MT can be calculated by dividing the heat exchange at the MT (figure 2) by the percentage of sample undergoing the MT. As shown in Figure 6b, although the cumulative errors are quite large, there is a significant and continuous enthalpy change reduction with the increase of milling time, which can be exclusively attributed to the presence of mechanically-induced defects (dislocations, antiphase boundaries…).

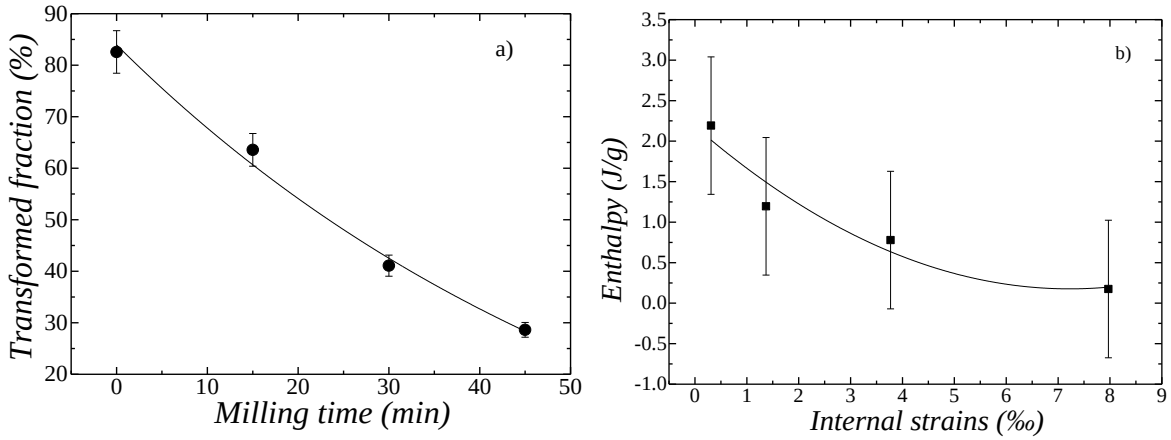

Figure 6. (a) Evolution of the volume fraction of the sample undergoing MT with the milling time of austenite. (b) Intrinsic transformation enthalpy as a function of the internal strains

Magnetic measurements have been carried out on the milled samples to correlate the microstructural state and the magnetic behavior. Figure 7 shows the temperature dependence of magnetization under low (100 Oe) and high (60 kOe) applied magnetic fields. In figure 7.a, a

clear magnetization jump associated with the ferro-paramagnetic transition takes place around 360 K in all samples except in the sample milled for 90 minutes. Likewise, at lower temperatures (around 175 K) the occurrence of the MT causes another magnetization drop, showing the characteristic thermal hysteresis. As in DSC thermograms, the MT is hardly detectable for milling times above 45 minutes. In all cases, the magnetization jumps become less sharp on increasing the milling time. However, both the Curie temperature of the austenite and the MT temperature remain almost constant irrespectively of the milling time, which, as previously mentioned, would indicate the absence of variations on the long-range atomic order. A remarkable decrease in the high-field magnetization change at the MT is observed, as expected from the gradual appearance of the mechanically-induced martensite and the NTRs. Besides, is worth noting that, comparing the measurements at 100 Oe and 60 kOe, the MT temperature shows approximately the same shift around 25 K to lower temperatures upon the application of high magnetic fields (see vertical lines).

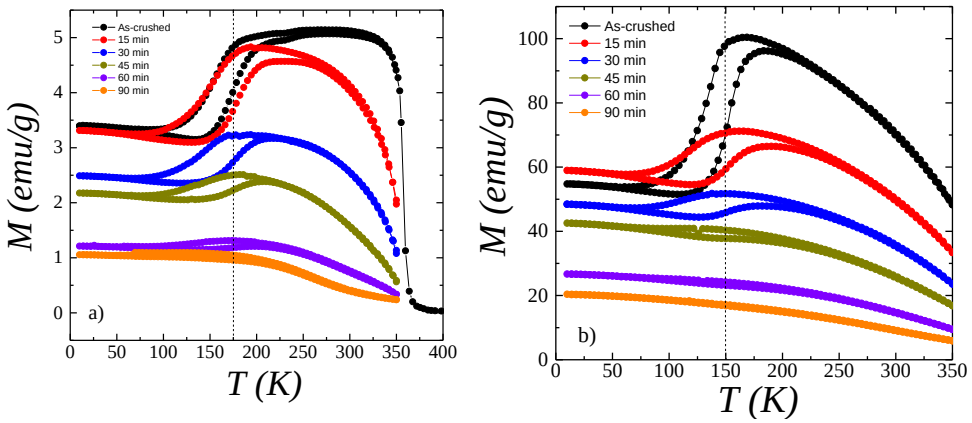

Figure 7. Temperature dependence of magnetization at (a) 100 Oe and (b) 60 kOe applied magnetic field.

In order to better analyze the effect of milling, the magnetic field dependence of the magnetization has been also measured at 10 K and 300 K. The obtained magnetization curves are shown in Figure 8. For milling times below 45 minutes, the magnetization drop is much more significant at high temperature (fig 8b), whereas a higher effect is observed at low temperature for longer milling times (fig 8a). In principle, this may be mainly attributed to the increasing amount of both martensite and NTR (showing very low magnetization) at high temperature and to the decrease of retained austenite at low temperature, respectively. In fact, the retained austenite increases with the milling time up to 30 minutes and then decreases (see figure 5). This austenite produces a high magnetic moment at low temperatures. Nevertheless, when the retained austenite decreases (above 30 minutes, see figure 5) the magnetization at low temperature also decreases noticeably as shown in figure 8a.

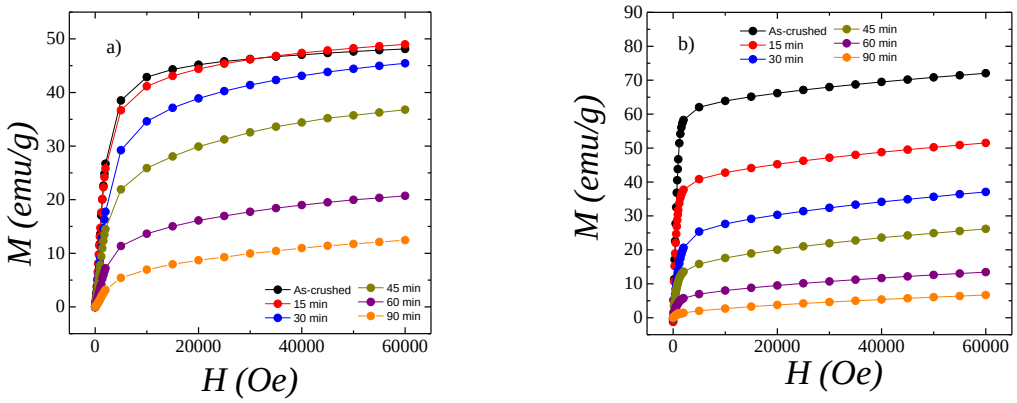

Figure 8. Isothermal magnetization as a function of the applied magnetic field at (a) 10 K and (b) 300 K.

The effect of the mechanical milling on the magnetization is clear from the evolution of magnetization at 60 kOe (M_{60kOe}) versus milling time, shown in Figure 9a. Despite the mixture of phases, if we compare this figure with Figure 5, it can be seen that M_{60kOe} at 300 K decreases in parallel with the austenite fraction. However, if we plot M_{60kOe} at 300 K versus the ausentite fraction at this temperature (Figure 9b), the evolution of magnetization with the austenite content lies far from a linear dependence, suggesting that other contributions, apart from the presence of martensite and NTR, must be considered to account for the evolution of the high-field magnetization. In order to better illustrate this, the magnetization corresponding just to the present phases has been estimated by using the expression $M_{Theo} = M_A P_A + M_M P_M + M_{NTR} P_{NTR}$, where M_A, M_M and M_{NTR} are the magnetization of austenite, martensite and NTR, respectively, and P_A, P_M and P_{NTR} are the corresponding percentages at 300K. If, in a first approximation, we consider M_M and M_{NTR} negligible over M_A (the martensite should be paramagnetic at 300 K and M_{60kOe} of the sample milled 90 minutes –in which more than the half of the mass consist on NTR- is close to just 5 emu/g), the magnetization can be then expressed as $M_{Theo} = M_A P_A$, where M_A is directly calculated from the experimental magnetization value and the austenite volume fraction at 300 K. A significative difference between the experimental and theoretical values of magnetization is observed in the figure, which can be therefore atributtable to the presence of the mechanically-induced defects.

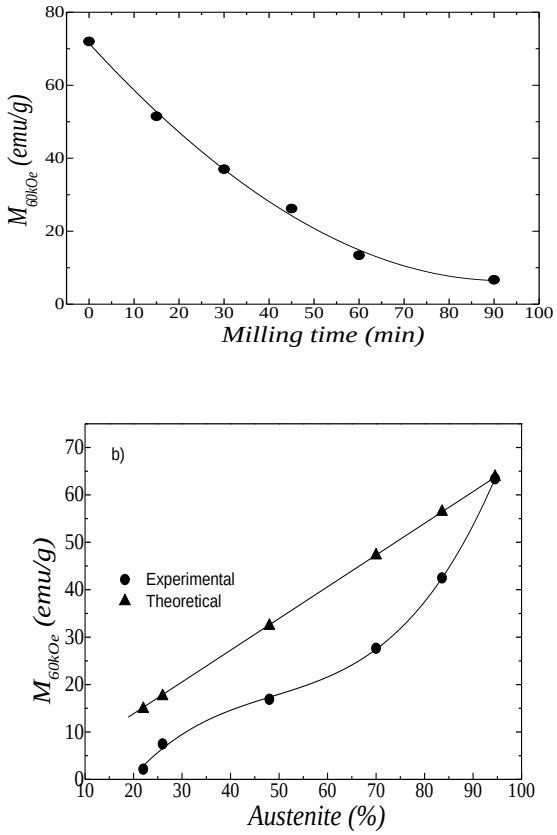

Figure 9. (a) Magnetization under 60 kOe at 300 K, as a function of the milling time. (b) Experimental and theoretical M_{60kOe} at 300 K as a function of the percentage of the austenitic phase. Lines are guides to the eyes.

The way defects affect the magnetization has been also analyzed by neutron diffraction in samples milled during 15, 30, and 45 minutes (see figure 10). The atoms site occupancies have been determined at 400 K (paramagnetic austenite) and the magnetic structure at 300 K (ferromagnetic austenite) by Rietveld method. The site occupancies for the austenitic $L2_1$ structure in all samples coincide with the previously reported for the as-crushed sample [41] (see Table I). As pointed out before, the long-range atomic order remains almost constant irrespectively of the milling time.

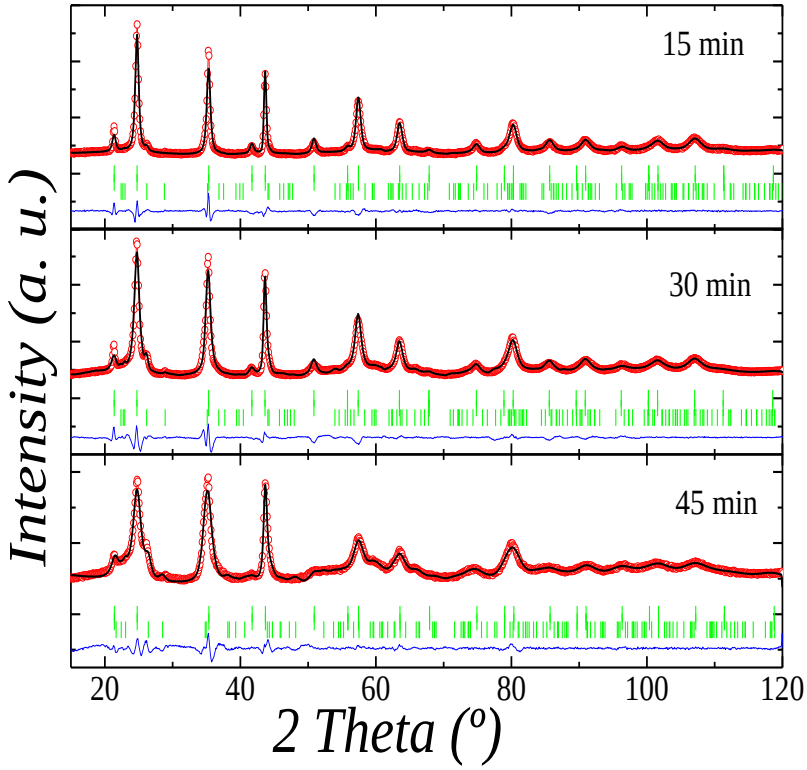

Figure 10. Experimental diffractograms at 300 K (red dots), calculated (black line) and the difference between experimental and calculated diffractograms (blue line) for the 15, 30 and 45 minutes milled alloys; the green marks indicate the Bragg reflections.

With respect to the magnetic structure, ferromagnetic coupling between the magnetic moment of Mn atoms in 4*a* and 4*b* sites is found in all samples (see Table I). However, the net magnetic moments of Mn atoms in the austenitic phase at 300 K significantly decrease with the increasing milling time, as shown in Figure 11a, This confirms again the influence of the microstructural defects of the magnetism, this time from a microscopic point of view. In fact, if we plot together the relative variation between theoretical and experimental magnetization, *(Mth-Mexp)/Mth*, and the relative variation on the magnetic moments as a function of the internal strains, a common behavior is observed.

Table I. Structural and magnetic parameters obtained from Rietveld refinement of the neutron diffraction data at 400 K and 300 K.

Samples	Sites				
	4*a*		4*b*		8*c**
	Occ	μ (μ_B)	Occ	μ (μ_B)	Occ
As-crushed [41]	0.94(2)Mn 0.06(1)Sn	3.11(2)	0.48(2)Mn 0.52(1)Sn	1.14(2)	0.88(3)Ni 0.12(1)Co
15 min	0.93(1)Mn 0.07(3)Sn	2.38(2)	0.47(3)Mn 0.53(2)Sn	0.76(9)	0.81(2)Ni 0.19(3)Co

30 min	0.95(3)Mn 0.05(1)Sn	2.16(3)	0.46(4)Mn 0.54(2)Sn	0.56(8)	0.88(2)Ni 0.12(3)Co
45 min	0.93(2)Mn 0.07(1)Sn	1.77 (1)	0.47(2)Mn 0.53(1)Sn	0.35(9)	0.92(2)Ni 0.08(2)Co

*The magnetic moments of Ni and Co in site *8c* are fixed to $0.2\mu_B$ and $1.0\mu_B$ respectively [37].

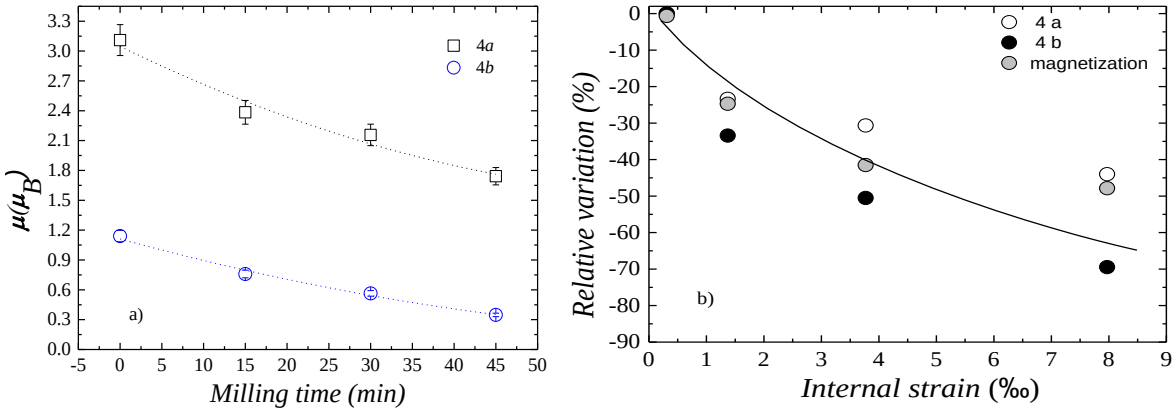

Figure 11. a) Evolution of the magnetic moments for 4*a* and 4*b* sites and b) normalized relative variation of both the magnetic moments obtained by Rietveld and the magnetization as a function of internal strains.

The obtained results thus confirm that ball-milling in a Ni45Co5Mn35Sn15 alloy give rise to an undesirable appearance of mechanically-induced martensite alongside with amorphous-like non-transforming regions. On the other hand, the mechanically- induced microstructural defects has been shown to cause a marked decrease in the magnetic moments of the Mn atoms. Therefore, upon the analyzed milling conditions, the mere use of ball-milling seems to be inadvisable for the production of potentially beneficial defects (as those found in hand-crushed samples). Subsequent annealing treatments could improve the martensitic transformation features and the magnetic properties. The study of the effect of post-milling thermal treatments will be the focus of further works.

Conclusions.

The effect of high-energy ball-milling on the magnetostructural properties of a $Ni_{45}Co_5Mn_{35}Sn_{15}$ alloy has been studied. A reduction of the particle size was found for samples milled until 45 minutes but for longer milling time the particle size increase due to the tendency to agglomerate and probably to a cold-welding effect. Moreover, the samples show an increase of the induced defects (internal strains) with the milling time which have been correlated with the variation of the magnetostructural properties; the intrinsic transformation enthalpy and the high field magnetization decrease with the internal strains probably linked to the presence of dislocations. On the other hand, the ball milling induces the transformation not only to

martensite but also to an amorphous-like structure (not transforming regions). A double stage has been observed during the milling process; at short times (below 30 minutes), a strong size reduction and martensite induction occurs. On the opposite, for longer times the strains increase predominates and consequently a larger amount of NTRs appear. Finally, the magnetic moment of Mn atoms at 4*a* and 4*b* position in austenite decreases with milling time but the ferromagnetic coupling persists.

Acknowledgments

This work has been carried out with the financial support of the Spanish "Ministerio de Economía y Competitividad" (Projects number MAT2015-65165-C2-R) "Agencia Estatal de Investigación (AEI), Ministerio de Ciencia, Innovación y Universidades" (Projects number RTI2018-094683-B-C54 (MCIU/AEI/FEDER, UE)), Navarra Government (Project number PC017-018 AMELEC) and Basque Government Grant No. IT-1005-16. We acknowledge ILL and ALBA for the beam time allocations: (http://doi.org/10.5291/ILL-DATA. INTER-411), CRG-2352, and ALBA BL04_MPSD beamline at ALBA Synchrotron with the collaboration of ALBA staff. PLR has received funding from "la Caixa" and "Caja Navarra" Foundations, under agreement LCF/PR/PR13/51080004.

Conflicts of Interest: The authors declare no conflict of interest

Bibliography.

[1] X. Moya, L. Manosa, A. Planes, T. Krenke, M. Acet, and E. F. Wassermann, "Martensitic transition and magnetic properties in Ni-Mn-X alloys," Mater. Sci. Eng. -Struct. Mater. Prop. Microstruct. Process. 438 (2006) 911–915. doi: 10.1016/j.msea.2006.02.053.

[2] R. Kainuma, Y. Imano, W. Ito, Y. Sutou, H. Morito, S. Okamoto, O. Kitakami, K. Oikawa, A. Fujita, T. Kanomata, and K. Ishida, "Magnetic-field-induced shape recovery by reverse phase transformation," Nature. 439 (2006) 957–960. doi: 10.1038/nature04493.

[3] K. Oikawa, W. Ito, Y. Imano, Y. Sutou, R. Kainuma, K. Ishida, S. Okamoto, O. Kitakami, and T. Kanomata, "Effect of magnetic field on martensitic transition of Ni46Mn41In13 Heusler alloy," Appl. Phys. Lett. 88 (2006) 122507. doi: 10.1063/1.2187414.

[4] T. Krenke, E. Duman, M. Acet, E. F. Wassemann, X. Moya, L. Mañosa, and A. Planes, "Inverse magnetocaloric effect in ferromagnetic Ni–Mn–Sn alloys," Nat. Mater. 4 (2005) 450–454. doi: 10.1038/nmat1395.

[5] J. Du, Q. Zheng, W. J. Ren, W. J. Feng, X. G. Liu, and Z. D. Zhang, "Magnetocaloric effect and magnetic-field-induced shape recovery effect at room temperature in ferromagnetic Heusler alloy Ni–Mn–Sb," J. Phys. Appl. Phys. 40 (2007) 5523. doi: 10.1088/0022-3727/40/18/001.

[6] R. Kainuma, Y. Imano, W. Ito, H. Morito, Y. Sutou, K. Oikawa, A. Fujita, K. Ishida, S. Okamoto, O. Kitakami, and T. Kanomata, "Metamagnetic shape memory effect in a Heusler-type Ni43Co7Mn39Sn11 polycrystalline alloy," Appl. Phys. Lett. 88 (2006) 192513. doi: 10.1063/1.2203211.

[7] R. Kainuma, W. Ito, R. Y. Umetsu, K. Oikawa, and K. Ishida, "Magnetic field-induced reverse transformation in B2-type NiCoMnAl shape memory alloys," Appl. Phys. Lett. 93 (2008) 091906. doi: 10.1063/1.2965811.

[8] V. D. Buchelnikov and V. V. Sokolovskiy, "Magnetocaloric effect in Ni-Mn-X (X= Ga, In, Sn, Sb) Heusler alloys," Phys. Met. Metallogr. 112 (2011) 633–665. doi: 10.1134/S0031918X11070052.

[9] D. Bourgault, J. Tillier, P. Courtois, D. Maillard, and X. Chaud, “Large inverse magnetocaloric effect in Ni45Co5Mn37.5In12.5 single crystal above 300 K,” Appl. Phys. Lett. 96 (2010) 132501. doi: 10.1063/1.3372633.
[10] S. Chatterjee, S. Giri, S. Majumdar, and S. K. De, “Giant magnetoresistance and large inverse magnetocaloric effect in Ni2Mn1.36Sn0.64alloy,” J. Phys. Appl. Phys.42 (2009) 065001. doi: 10.1088/0022-3727/42/6/065001.
[11] I. Dubenko, M. Khan, A. K. Pathak, B. R. Gautam, S. Stadler, and N. Ali, “Magnetocaloric effects in Ni–Mn–X based Heusler alloys with X=Ga, Sb, In,” J. Magn. Magn. Mater. 321 (2009) 754–757. doi: 10.1016/j.jmmm.2008.11.043.
[12] A. Ghosh and K. Mandal, “Large inverse magnetocaloric effect in Ni48.5−xCoxMn37Sn14.5 (x = 0, 1 and 2) with negligible hysteresis,” J. Alloys Compd. 579 (2013) 295–299. doi: 10.1016/j.jallcom.2013.06.062.
[13] A. K. Nayak, K. G. Suresh, and A. K. Nigam, “Giant inverse magnetocaloric effect near room temperature in Co substituted NiMnSb Heusler alloys,” J. Phys. Appl. Phys. 42(2009) 035009. doi: 10.1088/0022-3727/42/3/035009.
[14] M. Khan, A. K. Pathak, M. R. Paudel, I. Dubenko, S. Stadler, and N. Ali, “Magnetoresistance and field-induced structural transitions in Ni50Mn50−xSnx Heusler alloys,” J. Magn. Magn. Mater. 320 (2008) L21–L25. doi: 10.1016/j.jmmm.2007.06.016.
[15] A. K. Pathak, I. Dubenko, C. Pueblo, S. Stadler, and N. Ali, “Magnetoresistance and magnetocaloric effect at a structural phase transition from a paramagnetic martensitic state to a paramagnetic austenitic state in Ni50Mn36.5In13.5 Heusler alloys,” Appl. Phys. Lett. 96 (2010) 172503. doi: 10.1063/1.3422483.
[16] S. Singh and C. Biswas, “Magnetoresistance origin in martensitic and austenitic phases of Ni2Mn1+xSn1−x,” Appl. Phys. Lett. 98, 2011, 212101. doi: 10.1063/1.3592853.
[17] A. Çakır, L. Righi, F. Albertini, M. Acet, and M. Farle, “Intermartensitic transitions and phase stability in Ni50Mn50−xSnx Heusler alloys,” Acta Mater. 99 (2015) 140–149. doi: 10.1016/j.actamat.2015.07.072.
[18] T. Krenke, M. Acet, E. F. Wassermann, X. Moya, L. Mañosa, and A. Planes, “Ferromagnetism in the austenitic and martensitic states of Ni-Mn-In alloys,” Phys. Rev. B. 73 (2006) 174413. doi: 10.1103/PhysRevB.73.174413.
[19] T. Kanomata, T. Yasuda, S. Sasaki, H. Nishihara, R. Kainuma, W. Ito, K. Oikawa, K. Ishsida, K.U. Neumann, and K. R. A. Ziebeck., “Magnetic properties on shape memory alloys Ni2Mn1+xIn1−x,” J. Magn. Magn. Mater. 321 (2009) 773–776. doi: 10.1016/j.jmmm.2008.11.079.
[20] M. Khan, I. Dubenko, S. Stadler, and N. Ali, “Magnetostructural phase transitions in Ni50Mn25+xSb25-x Heusler alloys,” J. Phys. Condens. Matter. 20 (2008) 235204. doi: 10.1088/0953-8984/20/23/235204.
[21] A. Planes, L. Mañosa, and M. Acet, “Magnetocaloric effect and its relation to shape-memory properties in ferromagnetic Heusler alloys,” J. Phys. Condens. Matter. 21 (2009) 233201. doi: 10.1088/0953-8984/21/23/233201.
[22] T. Krenke, E. Duman, M. Acet, X. Moya, L. Mañosa, and A. Planes, “Effect of Co and Fe on the inverse magnetocaloric properties of Ni-Mn-Sn,” J. Appl. Phys. 102 (2007) 033903. doi: 10.1063/1.2761853.
[23] V. K. Sharma, M. K. Chattopadhyay, A. Khandelwal, and S. B. Roy, “Martensitic transition near room temperature and the temperature- and magnetic-field-induced multifunctional properties of Ni49CuMn34In16 alloy,” Phys. Rev. B. 82 (2010) 172411. doi: 10.1103/PhysRevB.82.172411.
[24] C. O. Aguilar-Ortiz, D. Soto-Parra, P. Álvarez-Alonso, P. Lázpita, D. Salazar, P. O. Castillo-Villa, H. Flores-Zúñiga, and V. A. Chernenko, “Influence of Fe doping and magnetic field on martensitic transition in Ni–Mn–Sn melt-spun ribbons,” Acta Mater. 107 (2016) 9–16. doi: 10.1016/j.actamat.2016.01.041.

[25] Z. Li, C. Jing, H. L. Zhang, Y. F. Qiao, S. X. Cao, J. C. Zhang, and L. Sun, “A considerable metamagnetic shape memory effect without any prestrain in Ni46Cu4Mn38Sn12 Heusler alloy,” J. Appl. Phys. 106 (2009) 083908. doi: 10.1063/1.3246809.
[26] V. Recarte, J. Pérez-Landazábal, V. Sánchez-Alarcos, and J. A. Rodriguez-Velamazán, “Dependence of the martensitic transformation and magnetic transition on the atomic order in Ni–Mn–In metamagnetic shape memory alloys,” Acta Mater. 60 (2012) 1937–1945. doi: 10.1016/j.actamat.2012.01.020.
[27] V. Recarte, J. I. Pérez-Landazábal, and V. Sánchez-Alarcos, “Dependence of the relative stability between austenite and martensite phases on the atomic order in a Ni–Mn–In Metamagnetic Shape Memory Alloy,” J. Alloys Compd. 536 (2012) S308–S311. doi: 10.1016/j.jallcom.2011.11.053.
[28] V. Sánchez-Alarcos, V. Recarte, J. I. Pérez-Landazábal, E. Cesari, and J. A. Rodríguez-Velamazán, “Long-Range Atomic Order and Entropy Change at the Martensitic Transformation in a Ni-Mn-In-Co Metamagnetic Shape Memory Alloy,” Entropy. 16 (2014) 2756–2767. doi: 10.3390/e16052756.
[29] J. López-García, V. Sánchez-Alarcos, V. Recarte, J. I. Pérez-Landazábal, O. Fabelo, E. Cesari, and J. A. Rodríguez-Velamazán, “Routes for enhanced magnetism in Ni-Mn-In metamagnetic shape memory alloys,” Scr. Mater. 167 (2019) 21–25. doi: 10.1016/j.scriptamat.2019.03.025.
[30] A. L. Alves, E. C. Passamani, V. P. Nascimento, A. Y. Takeuchi, and C. Larica, “Influence of grain refinement and induced crystal defects on the magnetic properties of Ni 50 Mn 36 Sn 14 Heusler alloy,” J. Phys. Appl. Phys. 43 (2010) 345001. doi: 10.1088/0022-3727/43/34/345001.
[31] I. Unzueta J. López-García, V. Sánchez-Alarcos, V. Recarte, J. I. Pérez-Landazábal, J. A. Rodríguez-Velamazán, J. S. Garitaonandia, J. A. García, and F. Plazaola, “119Sn Mössbauer spectroscopy for assessing the local stress and defect state towards the tuning of Ni-Mn-Sn alloys,” Appl. Phys. Lett. 110 (2017) 181908. doi: 10.1063/1.4982630.
[32] J. López-García, I. Unzueta, V. Sánchez-Alarcos, V. Recarte, J. I. Pérez-Landazábal, J. A. Rodríguez-Velamazán, J. A. García, and F. Plazaola, “Correlation between defects and magneto-structural properties in Ni-Mn-Sn metamagnetic shape memory alloys,” Intermetallics. 94 (2018) 133–137. doi: 10.1016/j.intermet.2017.12.028.
[33] P. Czaja, J. Przewoźnik, M. Fitta, M. Bałanda, A. Chrobak, B. Kania, P. Zackiewicz, A. Wójcik, M. Szlezynger, and M. Maziarz, “Effect of ball milling and thermal treatment on exchange bias and magnetocaloric properties of Ni48Mn39.5Sn10.5Al2 ribbons,” J. Magn. Magn. Mater. 401 (2016) 223–230. doi: 10.1016/j.jmmm.2015.10.043.
[34] A. Ghotbi Varzaneh, P. Kameli, V. R. Zahedi, F. Karimzadeh, and H. Salamati, “Effect of heat treatment on martensitic transformation of Ni47Mn40Sn13 ferromagnetic shape memory alloy prepared by mechanical alloying,” Met. Mater. Int. 21 (2015) 758–764. doi: 10.1007/s12540-015-4537-0.
[35] Y. Sutou, Y. Imano, N. Koeda, T. Omori, R. Kainuma, K. Ishida, and K. Oikawa, “Magnetic and martensitic transformations of NiMnX(X=In,Sn,Sb) ferromagnetic shape memory alloys,” Appl. Phys. Lett. 85 (2004) 4358–4360. doi: 10.1063/1.1808879.
[36] T. Krenke, M. Acet, E. F. Wassermann, X. Moya, L. Manosa, and A. Planes, “Martensitic transitions and the nature of ferromagnetism in the austenitic and martensitic states of Ni-Mn-Sn alloys,” Phys. Rev. B. 72 (2005) 014412. doi: 10.1103/PhysRevB.72.014412.
[37] Umetsu, R. Y, A. Sheikh, B. Ouladdiaf, K. R. A. Ziebeck, T. Kanomata, and R. Kainuma, “The effect of Co substitution on the magnetic properties of the Heusler alloy Ni50Mn33Sn17,” Appl. Phys. Lett. 98 (2011) 042507. doi: 10.1063/1.3548558.
[38] L. Huang, D. Y. Cong, H. L. Suo, and Y. D. Wang, “Giant magnetic refrigeration capacity near room temperature in Ni40Co10Mn40Sn10 multifunctional alloy,” Appl. Phys. Lett. 104 (2014) 132407. doi: 10.1063/1.4870771.
[39] V. Recarte, J. I. Pérez-Landazábal, S. Kustov, and E. Cesari, “Entropy change linked to the magnetic field induced martensitic transformation in a Ni–Mn–In–Co shape memory alloy,” J. Appl. Phys. 107 (2010) 053501. doi: 10.1063/1.3318491.

[40] V. Sánchez-Alarcos, J. I. Pérez-Landazábal, V. Recarte, I. Lucia, J. Vélez, and J. A. Rodríguez-Velamazán, "Effect of high-temperature quenching on the magnetostructural transformations and the long-range atomic order of Ni–Mn–Sn and Ni–Mn–Sb metamagnetic shape memory alloys," *Acta Mater.*, 61 (2013) 4676–4682. doi: 10.1016/j.actamat.2013.04.040.
[41] V. Sánchez-Alarcos, J. López-García, I. Unzueta, J. I. Pérez-Landazábal, V. Recarte, J. J. Beato-López, J. A. García, F. Plazaola, and J. A. Rodríguez-Velamazán, "Magnetocaloric effect enhancement driven by intrinsic defects in a Ni45Co5Mn35Sn15 alloy," J. Alloys Compd. 774 (2019) 86–592. doi: 10.1016/j.jallcom.2018.10.016..
[42] B. Tian, F. Chen, Y. X. Tong, L. Li, Y. F. Zheng, and Y. Liu, "The orientation dependence of transformation strain of Ni–Mn–Ga polycrystalline alloy and its composite with epoxy resin," J. Alloys Compd. 505 (2010) 680–684. doi: 10.1016/j.jallcom.2010.06.113.
[43] B. Tian, F. Chen, Y. X. Tong, L. Li, and Y. F. Zheng, "Bending properties of epoxy resin matrix composites filled with Ni–Mn–Ga ferromagnetic shape memory alloy powders," Mater. Lett. 63 (2009) 1729–1732. doi: 10.1016/j.matlet.2009.05.004.
[44] J. Feuchtwanger, M. L. Richard, Y. J. Tang, A. E. Berkowitz, R. C. O'Handley, and S. M. Allen, "Large energy absorption in Ni–Mn–Ga/polymer composites," J. Appl. Phys. 97 (2005) 10M319. doi: 10.1063/1.1857653.
[45] N. Scheerbaum, D. Hinz, O. Gutfleisch, K.-H. Müller, and L. Schultz, "Textured polymer bonded composites with Ni–Mn–Ga magnetic shape memory particles," Acta Mater. 55 (2007) 2707–2713. doi: 10.1016/j.actamat.2006.12.008.
[46] H. Hosoda, S. Takeuchi, T. Inamura, and K. Wakashima, "Material design and shape memory properties of smart composites composed of polymer and ferromagnetic shape memory alloy particles," Sci. Technol. Adv. Mater. 5 (2004) 503. doi: 10.1016/j.stam.2004.02.009.
[47] N. E. Barta and I. Karaman, "Embedded magnetic shape memory sensory particles in lightweight composites for crack detection," *Mater. Sci. Eng. A*, 751 (2019) 201–213. doi: 10.1016/j.msea.2019.01.076.
[48] A. Mostafaei, P. Rodriguez De Vecchis, E. L. Stevens, and M. Chmielus, "Sintering regimes and resulting microstructure and properties of binder jet 3D printed Ni-Mn-Ga magnetic shape memory alloys," Acta Mater. 154 (2018) 355–364. doi: 10.1016/j.actamat.2018.05.047.
[49] M. P. Caputo, A. E. Berkowitz, A. Armstrong, P. Müllner, and C. V. Solomon, "4D printing of net shape parts made from Ni-Mn-Ga magnetic shape-memory alloys," Addit. Manuf. 21 (2018) 579–588. doi: 10.1016/j.addma.2018.03.028.
[50] S. L. Taylor, R. N. Shah, and D. C. Dunand, "Ni-Mn-Ga micro-trusses via sintering of 3D-printed inks containing elemental powders," Acta Mater. 143 (2018) 20–29. doi: 10.1016/j.actamat.2017.10.002.
[51] M. Sopicka-Lizer, High-Energy Ball Milling: Mechanochemical Processing of Nanopowders. Elsevier, 2010.
[52] A. L. Alves, A. Magnus Gomes Carvalho, J. R. Cápua Proveti, V. P. Nascimento, and E. C. Passamani, "EXAFS studies of enhancement of L21-B2 chemical disorder induced by ball milling in martensitic Ni50Mn36Sn14 pseudo-Heusler alloy," Mater. Charact. 158 (2019) 109972. doi: 10.1016/j.matchar.2019.109972.
[53] C. A. Schneider, W. S. Rasband, and K. W. Eliceiri, "NIH Image to ImageJ: 25 years of image analysis," Nat. Methods. 9 (2012) 671–675. doi: 10.1038/nmeth.2089.
[54] F. Fauth, I. Peral, C. Popescu, and M. Knapp, "The new Material Science Powder Diffraction beamline at ALBA Synchrotron," Powder Diffr. 28 (2013) S360–S370. doi: 10.1017/S0885715613000900.
[55] I. Peral, J. McKinlay, M. Knapp, and S. Ferrer, "Design and construction of multicrystal analyser detectors using Rowland circles: application to MAD26 at ALBA," J. Synchrotron Radiat. 18, (2011) 842–850. doi: 10.1107/S0909049511031529.
[56] J. Rodríguez-Carvajal, "Recent advances in magnetic structure determination by neutron powder diffraction," Phys. B Condens. Matter. 192 (1993) 55–69. doi: 10.1016/0921-4526(93)90108-I.

[57] E. Sakher, N. Loudjani, M. Benchiheub, and M. Bououdina, “Influence of Milling Time on Structural and Microstructural Parameters of Ni50Ti50 Prepared by Mechanical Alloying Using Rietveld Analysis,” J. Nanomater. 2018 (2018) 2560641. doi: 10.1155/2018/2560641.
[58] B. Tian, Y. X. Tong, F. Chen, L. Li, and Y. F. Zheng, “Effect of aging and ball milling on the phase transformation of Ni50Mn25Ga17Cu8−xZrx alloys,” Intermetallics. 58 (2015) 56–61. doi: 10.1016/j.intermet.2014.11.007.
[59] R. Kainuma, F. Gejima, Y. Sutou, I. Ohnuma, and K. Ishida, “Ordering, Martensitic and Ferromagnetic Transformations in Ni–Al–Mn Heusler Shape Memory Alloys,” *Mater. Trans. JIM*, 41 (2000), 943–949. doi: 10.2320/matertrans1989.41.943.
[60] P. Entel, V. D. Buchelnikov, M. E. Gruner, A. Hucht, V. V. Khovailo, S. K. Nayak, and A. T. Zayakm, “Shape Memory Alloys: A Summary of Recent Achievements,” *Materials Science Forum*, 583, (2008), 21-41. doi: 10.4028/www.scientific.net/MSF.583.21.